FEBS Letters

FEBS PRESS science publishing by scientists

COMMUNICATION

Crystal structure of a NADPH-cytochrome P450 oxidoreductase (CYPOR) and heme oxygenase 1 fusion protein implies a conformational change in CYPOR upon NADPH/NADP$^+$ binding

Masakazu Sugishima[1], Hideaki Sato[1], Kei Wada[2] and Ken Yamamoto[1]

1 Department of Medical Biochemistry, Kurume University School of Medicine, Kurume, Japan
2 Department of Medical Sciences, University of Miyazaki, Miyazaki, Japan

Correspondence
M. Sugishima, Department of Medical Biochemistry, Kurume University School of Medicine, 67 Asahi-machi, Kurume, Fukuoka 830-0011, Japan
Tel: +81 942 31 7544
E-mail: sugishima_masakazu@med.kurume-u.ac.jp

(Received 12 February 2019, revised 6 March 2019, accepted 12 March 2019, available online 25 March 2019)

doi:10.1002/1873-3468.13360

Edited by Miguel De la Rosa

Heme oxygenase-1 (HMOX1) catalyzes heme degradation utilizing reducing equivalents supplied from NADPH-cytochrome P450 reductase (CYPOR). Recently, we determined the complex structure of NADP$^+$-bound open-conformation stabilized CYPOR and heme-HMOX1, but the resolution was limited to 4.3 Å. Here, we determined the crystal structure of the fusion protein of open-conformation stabilized CYPOR and heme-HMOX1 at 3.25 Å resolution. Unexpectedly, no NADP$^+$ was bound to this fusion protein in the crystal. Structural comparison of the NADP$^+$-bound complex and the NADP$^+$-free fusion protein suggests that NADP$^+$ binding regulates the conformational change in the FAD-binding domain of CYPOR. As a result of this change, the FMN-binding domain of CYPOR approaches heme-bound HMOX1 upon NADP$^+$ binding to enhance the electron-transfer efficiency from FMN to heme.

Keywords: electron transfer; protein–protein interaction; conformation change; X-ray crystallography

Heme oxygenase (HMOX; EC 1.14.11.18) catalyzes the degradation of heme to biliverdin, carbon monoxide (CO), and ferrous ion by utilizing reducing equivalents supplied from NADPH-cytochrome P450 oxidoreductase (CYPOR; EC 1.6.2.4) [1–3], with biliverdin subsequently converted to bilirubin by biliverdin reductase (EC 1.3.1.24). The major physiological roles of HMOX in mammals are assigned to an inducible isoform (HMOX1) and include iron recycling, heme detoxification (as a pro-oxidant), and bilirubin production (as a potent antioxidant). CO produced by HMOX1 and a constitutive isoform (HMOX2) mediates various types of cell signaling, including that associated with anti-inflammation, antiapoptosis, and vasodilatation [4,5].

The CYPOR is a member of a family of diflavin reductases that includes methionine synthase reductase (EC 1.16.1.8), the reductase domains of nitric oxide synthase (EC 1.14.13.39) and cytochrome P450 BM3 (EC 1.14.14.1), and the flavoprotein subunit of sulfite reductase (EC 1.8.1.2). The electron flux from NADPH to the redox partner of CYPOR follows a linear pathway: NADPH→FAD→FMN→heme in the redox partner. The FAD accepts two electrons and one proton as a hydride from NADPH, and the FMN acts as a one-electron carrier [6–8]. The CYPOR structure comprises

Abbreviations
CYPOR, NADPH-cytochrome P450 oxidoreductase; heme-rHMOX1, rat HMOX1 in complex with heme; heme-rHMOX1–ΔTGEE, heme-bound rHMOX1–ΔTGEE; HMOX, heme oxygenase; rHMOX1–ΔTGEE, fusion of rat HMOX1 and ΔTGEE; TCA, trichloroacetic acid; ΔTGEE: heme-rHMOX1, complex of ΔTGEE with heme-rHMOX1; ΔTGEE, rat CYPOR mutant to keep the open conformation.

three domains: an FMN-containing flavodoxin-like domain, a ferredoxin-$NADP^+$ oxidoreductase (FNR)-like domain, and the domain connecting the two former domains. The connecting domain and the FNR-like domain form the FAD-binding domain, where the $NADPH/NADP^+$-binding site resides. The FAD- and FMN-binding domains are connected by a flexible hinge spanning 12 amino acid residues (Gly232 to Arg243) in rat CYPOR. For electron transfer to occur, association is required between CYPOR and its redox partners. Recently, we determined the crystal structure of the complex of rat CYPOR in its stabilized open conformation (ΔTGEE; deletion of residues Thr236 to Glu239) [9] and heme-bound rat HMOX1 (heme-rHMOX1) at 4.3 Å resolution [10,11]. The structure showed FMN located near the heme group, thereby enabling electron transfer from FMN to the heme; however, the distance between FAD and FMN was > 20 Å, suggesting that rapid electron transfer from FAD to FMN would be difficult if the structure is maintained during the entire electron-transfer process. To complete the cycle of the HMOX reaction, HMOX consumes seven electrons provided by CYPOR. The wild-type rat CYPOR structure shows a closed conformation, in which $NADP^+$, FAD, and FMN are located in close proximity, thereby making this conformation suitable for intramolecular electron transfer [12]. Therefore, this suggests that a 'closed–open transition' of CYPOR that includes HMOX association and dissociation must occur during the HMOX reaction [10].

To improve crystallographic resolution of the complex structure, we constructed a fusion protein of rat HMOX1 and ΔTGEE (rHMOX1–ΔTGEE) based on the complex structure and crystallized the fusion protein in complex with heme. Unexpectedly, we found that $NADP^+$ was not bound to the fusion protein in the crystal. Based on our findings, we propose the presence of a conformation change in CYPOR associated with $NADPH/NADP^+$ binding.

Materials and methods

Preparation of fusion enzymes

In the crystal structure of the ΔTGEE:heme-rHMOX1 complex (PDB ID: 3WKT), the distances between the C terminus (Glu223) of rat HMOX1 and the N terminus (Glu66) of ΔTGEE and between the C terminus (Ser674) of ΔTGEE and the N terminus (Ser10) of rat HMOX1 are similar (36 Å). However, the presence of a linker between the C terminus of ΔTGEE and the N terminus of rat HMOX1 might prevent an interaction between HMOX1 and ΔTGEE based on the location of the linker relative to the FAD-binding and FMN-binding domains of ΔTGEE. Therefore, we prepared fusion proteins with HMOX1 and ΔTGEE located on the N-terminal and C-terminal regions, respectively. Moreover, we prepared three types of fusion constructs with variable linker lengths between HMOX1 and ΔTGEE (13, 15, and 17 residues). The linker sequences originated from the rat HMOX1 sequence (from Thr222 to Thr233, Phe235, or Arg237), and a methionine residue was added at the last residue of the linker. To disrupt the helix located at the C terminus of HMOX1, Thr222 was substituted with a proline residue in all constructs (Fig. 1). Pro230 was also substituted with alanine to increase the flexibility of the linker.

We used an In-Fusion HD cloning kit (Takara Bio, Shiga, Japan) to construct the expression system for the fusion proteins. The expression plasmid containing N-terminal 6 × His-tagged rat HMOX1 (pET15b-rat HMOX1; previously constructed [13]) was linearized by PCR with primers 1 and 2-13aa (Table 1). Mutation of P230A was also introduced by this PCR reaction. The open reading frame (ORF) region was amplified by PCR from the expression plasmid for ΔTGEE using primers 3 and 4 (Table 1). The linearized vector containing *hmox1* was then

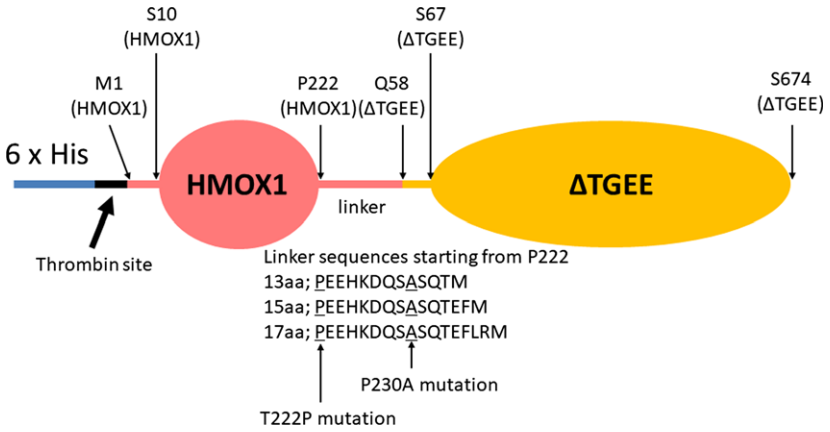

Fig. 1. Construct of the rHMOX1–ΔTGEE fusion protein. Schematic diagram of the domain construct of the rHMOX1–ΔTGEE fusion protein. Filled circles show the visible regions in the crystal structures. The His-tag, protease cleavage site, and amino acid sequences of the linker are shown.

Table 1. Primer sequences.

1	CTCGAGGATCCGGCTGCTA
2-13aa	TGTCTGTGAGGCACTCTGGTCTTTG
3	**AGTGCCTCACAGACA**ATGCAAACAACGGCCCCA
4	**AGCCGGATCCTCGAG**CTAGCTCCACACATCTAGT
T222P-f	CTGCCAGAGGAACACAAAGACC
T222P-r	CAGTGCCTGCAGCTCCTC
15aa-f	GAATTTATGCAAACAACGGCCCCACCCGTC
17aa-f	GAATTTCTGCGTATGCAAACAACGGCCCCACC

Sequences used for mutations or insertions are underlined. Sequences used for in-fusion reactions are in bold.

fused with *ΔTGEE* according to manufacture protocol, and sequences of the ORF regions in the resulting plasmids were verified. T222P mutation and insertion along with the 15aa and 17aa linkers were carried out using a KOD site-directed mutagenesis kit (Toyobo, Osaka, Japan) using primers T222P-f, T222P-r, 2-13aa, 15aa-f, and 17aa-f (Table 1).

Fusion proteins were all expressed in *Escherichia coli* BL21 (DE3) cells (Merck, Burlington, MA, USA) at 30 °C using Terrific-Broth media without isopropyl β-D-1-thiogalactopyranoside induction, and fusion proteins were purified from the soluble extracts of each overexpressed culture. Because the 6 × His-tag was attached at the N terminus in all expressed fusion proteins, they were purified using Ni-NTA agarose HP resin (Wako Pure Chemical Industries, Ltd., Osaka, Japan) according to manufacturer protocol, followed by additional purification with 2′,5′-ADP sepharose (GE Healthcare, Little Chalfont, UK) and hydroxyapatite (CHT-I; Bio-Rad Laboratories, Hercules, CA, USA) columns, as reported previously [14]. $NADP^+$ was used for elution of the fusion proteins from the sepharose column. Typical yields of these fusion proteins were 100 mg from 0.6 L culture medium.

Size-exclusion chromatography

Each purified 6 × His-tagged rHMOX1–ΔTGEE fusion was mixed with hemin at a molar ratio of 1 : 5 at 4 °C and incubated overnight. The mixture then was applied to a Superdex 200 10/300 GL column connected to an ÄKTAprime plus system (GE Healthcare) following column equilibration with 20 mM Tris-HCl buffer (pH 7.4). Proteins were eluted with the same buffer, and absorbance at 280 nm was recorded.

Crystallization and structure determination

Each monomer and oligomer fraction of the fusion protein was concentrated to 40 $mg{\cdot}mL^{-1}$ by ultrafiltration using Amicon Ultra (Merck). Crystallization conditions were screened at 20 °C by sitting-drop vapor diffusion using a JB Classic screening kit (Jena Bioscience, Jena, Germany). Plate-shaped orange crystals of the heme-rHMOX1–ΔTGEE fusion protein were obtained from the oligomer fraction at 20 °C in reservoir solution containing 10% (w/v) PEG 20000 and 0.1 M MES-NaOH (pH 6.5). The length of the linker had no apparent effect in crystallization. We ultimately optimized the reservoir conditions to 8% (w/v) PEG 20000, 0.1 M MES-NaOH (pH 6.0), and 0.5% ethyl acetate. Crystals were soaked in crystallization solution containing PEG 20000 up to 10% (w/v), 10% (v/v) ethylene glycol, and 10% (w/v) sucrose for cryopreservation, followed by introduction of liquid nitrogen. Diffraction data were collected at 100 K using synchrotron radiation at beamline BL44XU (SPring-8, Sayo, Japan; Proposal Nos. 2016AB6622, 2016A6700, 2017B6725, 2017AB6765, 2017A6766, and 2018AB6700), with the wavelength of the X-ray used for structure refinement at 0.9 Å. Diffraction data were processed, merged, and scaled using the XDS package [15] for the 13aa-linker variant and HKL2000 [16] for the 15aa- and 17aa-linker variants. Crystallographic statistics are summarized in Table 2.

Protein phases were determined by molecular replacement with Molrep [17,18] using the complex structure of ΔTGEE:heme-rHMOX1 (PDB ID: 3WKT) as a search model. The model was further refined with Phenix and adjusted with Coot [18–20]. During refinement, non-crystallographic symmetry restraints between two fusion proteins in an asymmetric unit were applied. Stereochemical evaluation of the models was performed with the program MOLPROBITY [21]. Diffraction and refinement statistics are summarized in Table 2. The coordinates and structure factors have been deposited in the Protein Data Bank with accession codes 6J79 (13aa), 6J7I (15aa), and 6J7A (17aa).

High-performance liquid chromatography analysis

To determine $NADP^+$ content in the fusion protein, $NADP^+$ and other coenzymes were extracted from purified ΔTGEE or the fusion protein by trichloroacetic acid (TCA) precipitation. The supernatants were immediately diluted 10-fold with running buffer [0.15 M sodium phosphate/citrate buffer (pH 6.8) containing 1 mM EDTA] and analyzed according to the same procedures reported by Aso *et al.* [22], except for use of a different column (4.6 × 250 mm^2; InertSustainSwift C18 column; GL Sciences, Tokyo, Japan) connected to a Waters Alliance e2695 HPLC and 2998 PDA detector system (Waters, Milford, MA, USA).

Results and Discussion

Properties of the heme-rHMOX1–ΔTGEE fusion protein

We expressed and purified the rHMOX1–ΔTGEE fusion protein, with size-exclusion chromatography demonstrating its status as a monomer. However, upon the addition of excess amounts of hemin, we

Table 2. Crystal structure statistics for data collection and structure refinement.

Crystallographic dataset	13aa	15aa	17aa
Wavelength (Å)	0.9000	0.9000	0.9000
Space group	$P2_12_12_1$	$P2_12_12_1$	$P2_12_12_1$
Unit cell (*a, b, c;* Å)	83.4, 159.8, 189.6	83.2, 158.2, 189.2	82.4, 159.6, 189.2
Diffraction statistics[a]			
Maximum resolution (Å)	3.33 (3.42–3.33)	3.30 (3.36–3.30)	3.25 (3.31–3.25)
Redundancy	8.1 (7.6)	3.3 (3.1)	3.7 (3.4)
Completeness (%)	99.0 (91.4)	91.6 (88.6)	96.3 (97.0)
Mean $I_\sigma/\sigma(I)$	14.0 (1.9)	10.9 (2.0)	13.1 (1.8)
R_{sym}[b] (%)	9.6 (118.3)	10.8 (71.5)	8.8 (63.6)
Refinement statistics			
R-factor[c] (%)	20.2	19.2	22.8
R_{free}[d] (%)	24.9	24.1	24.6
Number of atoms			
Protein/ligands/water	13 075/254/16	13 075/254/0	13 016/254/3
Average B-factors (Å^2)			
Protein/ligands/water	129.7/113.7/82.2	65.1/44.9/none	73.7/56.4/30.6
Rms deviations from ideal values			
Bond lengths (Å)	0.002	0.005	0.002
Bond angles (degree)	0.641	0.727	0.662
Ramachandran plot			
Preferred (%)	92.9	93.7	94.3
Allowed	6.6	5.9	5.3
Disallowed (%)	0.5	0.4	0.4
PDB ID	6J79	6J7I	6J7A

[a] Values in parentheses correspond to the highest resolution shell.
[b] $R_{sym} = \sum_{hkl}\sum_i |I_i(hkl) - <I(hkl)>| / \sum_{hkl}\sum_i I_i(hkl)$.
[c] *R*-factor $= \sum_{hkl}||F_o(hkl)| - |F_c(hkl)|| / \sum_{hkl}|F_o(hkl)|$.
[d] R_{free} is the *R*-factor calculated for 5% of the data not included in the refinement.

observed oligomerization of a portion of the fusion protein (Fig. 2A). The UV-visible absorption spectrum of the oligomer fraction showed a clear absorption peak at 410 nm (Soret band), indicating heme binding (Fig. 2B). Subsequent treatment of the oligomer fraction with thrombin digestion to remove the N-terminal 6 × His-tag resulted in monomerization (Fig. 2A). Therefore, this suggested that the 6 × His-tag and hemin were involved in oligomerization likely due to the weak binding of hemin to the 6 × His-tag. This was also supported by the absence of oligomer formation following addition of an equimolar amount of hemin. We have not tested the enzymatic activities of these fusion proteins but basically these must be inactive because the ΔTGEE mutation fixes the conformation of the CYPOR part of the fusion protein to open. In the open conformation of CYPOR, the distance between FAD and FMN is too long for the electron transfer between them [10]. As shown below, the distances between FAD and FMN in the fusion proteins are too long as in ΔTGEE:heme-rHMOX1 complex.

A previous study reported that the K_d of human CYPOR for $NADP^+$ is 53 nM according to calorimetric analysis [23], suggesting that $NADP^+$ is usually tightly bound to CYPOR. To confirm $NADP^+$ binding to the fusion protein, we performed HPLC analysis, followed by TCA precipitation. In the sample solution that was passed through the size-exclusion column equilibrated with $NADP^+$-free buffer, we found that $NADP^+$ was present at almost equimolar concentrations with the 13aa-linker fusion protein (Fig. 3). That implied $NADP^+$ was bound to the purified fusion protein before crystallization.

Crystal structure of the heme-rHMOX1–ΔTGEE fusion protein

We screened the crystallization conditions for both the oligomer and monomer fractions of the heme-bound 6 × His-tagged rHMOX1–ΔTGEE fusion protein, and found that only the oligomer fraction was able to crystallize under conditions that differed from those of the ΔTGEE:heme-rHMOX1 complex [10]. Moreover, the space group and crystal lattices of the fusion-protein crystal also differed from those of the original complex (Table 2).

Although we were able to crystallize the oligomer fraction, the structure of the fusion protein appeared to

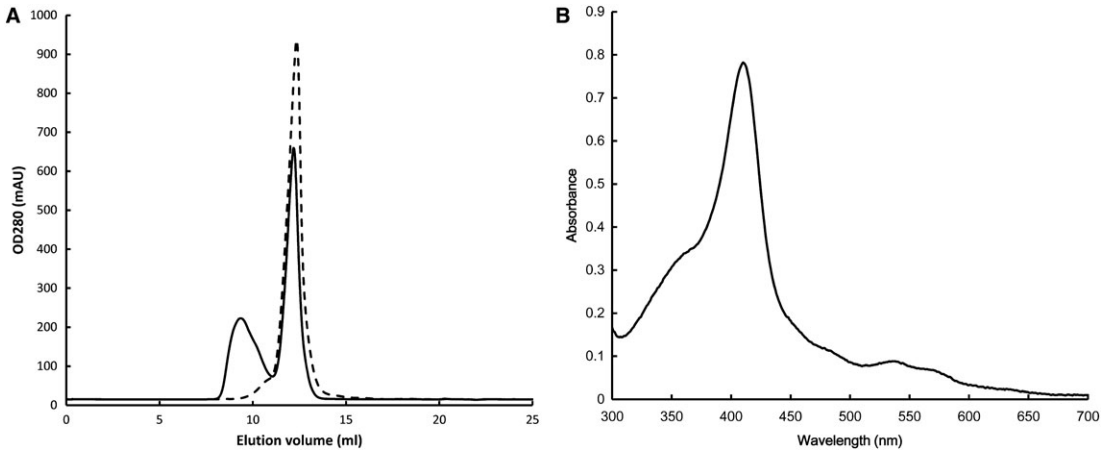

Fig. 2. Size-exclusion chromatograms of the rHMOX1–ΔTGEE fusion protein in complex with heme. (A) Solid and broken lines show chromatograms before and after 6 × His-tag cleavage, respectively. Elution peaks at 9.5 mL and at 12 mL represent the oligomer and monomer forms, respectively. (B) UV–visible spectrum of the oligomer fraction. The oligomer is solved in the 0.1 M potassium phosphate buffer (pH 7.4).

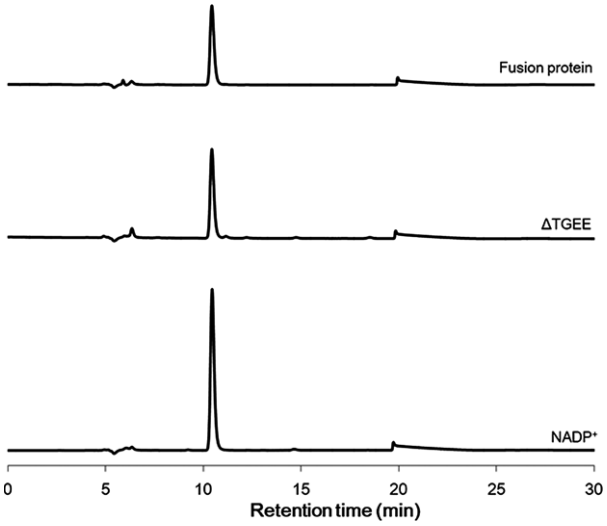

Fig. 3. High-performance liquid chromatography chromatograms of supernatants containing the 13aa-linker–ΔTGEE fusion protein treated with TCA precipitation. Chromatograms recorded at 260 nm. The peak eluted at 10.4 min contains $NADP^+$. Extracts from 0.81 nmol protein or 0.8 nmol $NADP^+$ were applied to the column. $NADP^+$ bound in the fusion protein was almost identical amount to that present in the ΔTGEE variant. Detailed elution conditions are described in the Materials and Methods section.

be monomeric. The linker region was disordered, indicating the lack of a stable conformation in this variant. Therefore, this suggested that the linker would not prevent the interaction between ΔTGEE and heme-rHMOX1. Additionally, linker lengths of at least 13aa to 17aa did not affect the conformation of the fusion protein. Unless otherwise stated, the structure of the fusion protein described here contained a 17aa linker, as that variant allowed a structure with the best resolution. To compare the residue numbers of the fusion proteins with those of the ΔTGEE:heme-rHMOX1 complex, we described the residue number of the fusion protein according to the corresponding numbers in ΔTGEE or HMOX1. Notably, the residue numbers of the fusion proteins deposited in the PDB differ from those described in this paper (i.e., Gln58 of ΔTGEE was recorded as Gln235 for the 13aa-fusion protein, Gln237 for the 15aa-fusion protein, and Gln239 for the 17aa-fusion protein in the PDB, respectively). Compared with the previous structure of the ΔTGEE:heme-rHMOX1 complex, present fusion-protein structure showed an improved crystallographic resolution from 4.3 Å to 3.25 Å. Despite overall similarity between the fusion protein and the previously reported complex, $NADP^+$ was not bound by the fusion protein (Fig. 4A). As showing in Fig. 3, $NADP^+$ was copurified with the fusion protein. Also $NADP^+$ was bound to ΔTGEE during the similar purification procedure [10]. These implied that $NADP^+$ was bound to the fusion protein during the purification step involving the 2′,5′-ADP sepharose column as well as ΔTGEE and $NADP^+$ was subsequently released from the fusion protein upon crystallization. Compared with the structure of the ΔTGEE:heme-rHMOX1 complex, the loop between Gly627 and Asn631 (corresponding to Gly631 and Asn635 in the wild-type CYPOR structure based on the deletion of four residues from Thr236 to Glu239 in ΔTGEE) was flipped due to electrostatic repulsion between Asp628 (Asp632 in the wild-type CYPOR) and the negative charge of the pyrophosphate group of $NADP^+$. Xia *et al.* [24]

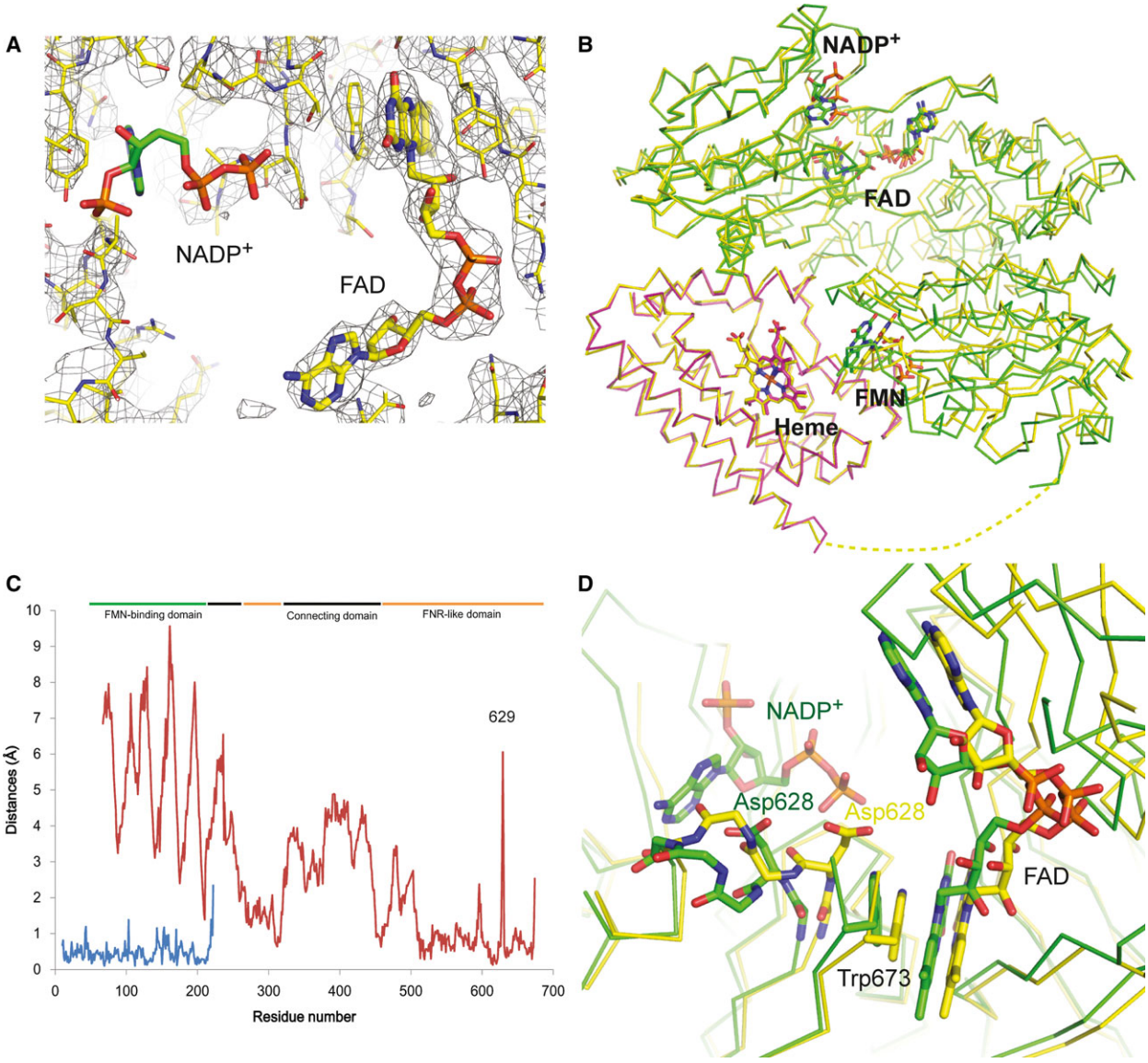

Fig. 4. Crystal structure of the NADP$^+$-free heme-rHMOX1–ΔTGEE fusion protein. Superimposition of the NADP$^+$-bound complex of ΔTGEE:heme-rHMOX1 onto the NADP$^+$-free fusion protein was performed to minimize root-mean-square deviations in the HMOX1 region of each model. (A) NADP$^+$- and FAD-binding sites. The $2F_o-F_c$ map of the NADP$^+$-free fusion protein contoured by 1.3 σ superimposed onto the fusion-protein model (yellow). Superimposition of the NADP$^+$ from the model of the ΔTGEE:heme-rHMOX1 complex. No corresponding electron density for NADP$^+$ was observed in the fusion protein. (B) Superimposition of the NADP$^+$-free fusion protein (yellow) onto the NADP$^+$-bound ΔTGEE (green)–heme-rHMOX1 (pink) complex. The invisible linker region in the fusion protein is illustrated as a broken line. (C) Plot of the distances between Cα atoms in the fusion protein and the ΔTGEE:heme-rHMOX1 complex. Blue and red lines show the distances within the HMOX1 and ΔTGEE regions, respectively. Solid horizontal bars indicate the domains in the ΔTGEE variant. (D) Close-up view of the NADP$^+$- and FAD-binding sites in (B). Stick models of NADP$^+$, FAD, Trp673, and the flipped loop between Gly627 and Asn631. For clarity, side chains in the flipped loop (except for Asp628) are not shown.

reported the introduction of an artificial disulfide bridge into the structure of NADP$^+$-free CYPOR in order to maintain a closed conformation. The structural difference between the NADP$^+$-bound ΔTGEE:heme-rHMOX1 complex [10] and NADP$^+$-free fusion protein was similar that reported previously in the vicinity of the NADP$^+$-binding site. Although the NADP$^+$-dependent change in conformation was limited in the vicinity of the NADP$^+$-binding site in the closed conformation of CYPOR reported previously [24], we observed that the conformation change spread toward the FMN-binding domain in the open conformation of

CYPOR (Fig. 4B,C). When $NADP^+$ was bound, the flipping motion of the Asp628 side chain pulled the flavin ring of FAD through a pi-stacking conformation along with Trp673 (Fig. 4D). This motion was then transmitted throughout the connecting and FMN-binding domains (Fig. 4C), resulting in a narrowing of the HMOX-binding cleft of ΔTGEE in order to adapt to the shape of HMOX1 and move FMN toward the heme group upon $NADP^+$ binding (Fig. 4B). We found that the shortest distance between FMN and the heme group changed from 8.0 Å ($NADP^+$-free fusion protein) to 5.7 Å ($NADP^+$-bound complex) although the distance between FMN and FAD did not largely change. The change in the distance between FMN and the heme group suggests that this activity might enhance the efficiency of electron transfer from CYPOR to the heme-rHMOX1 complex upon NADPH/$NADP^+$ binding.

Acknowledgements

We thank the staff at beamline BL44XU at SPring-8 for their assistance with data collection. We also thank Prof. Hiroshi Sakamoto and Dr. Junichi Taira of Kyushu Institute of Technology, and Prof. Yuichiro Higashimoto of Kurume University School of Medicine for their helpful discussions. This work was partially supported by JSPS KAKENHI (grant Nos. 16K07280 and 25840026), by grants from the Takeda Science Foundation and the Protein Research Foundation to MS and KW, and by the Platform Project for Supporting Drug Discovery and Life Science Research [Basis for Supporting Innovative Drug Discovery and Life Science Research (BINDS)] from AMED (grant Nos. JP17am0101072 and JP18am0101072).

Author Contributions

MS designed fusion protein constructs, prepared these proteins, and analyzed all data. MS and HS analyzed HPLC experiments. MS, HS, and KW performed X-ray experiments. MS, HS, KW, and KY wrote and revised the manuscript and discussed the structure-function relationship.

References

1 Kikuchi G, Yoshida T and Noguchi M (2005) Heme oxygenase and heme degradation. *Biochem Biophys Res Commun* **338**, 558–567.

2 Ortiz de Montellano PR and Wilks A (2001) Heme oxygenase structure and mechanism. In *Advances in Inorganic Chemistry* (Sykes AG, ed.), pp. 359–407. Academic Press, San Diego.

3 Tenhunen R, Marver HS and Schmid R (1968) The enzymatic conversion of heme to bilirubin by microsomal heme oxygenase. *Proc Natl Acad Sci USA* **61**, 748–755.

4 Ryter SW, Alam J and Choi AM (2006) Heme oxygenase-1/carbon monoxide: from basic science to therapeutic applications. *Physiol Rev* **86**, 583–650.

5 Morikawa T, Kajimura M, Nakamura T, Hishiki T, Nakanishi T, Yukutake Y, Nagahata Y, Ishikawa M, Hattori K, Takenouchi T *et al.* (2012) Hypoxic regulation of the cerebral microcirculation is mediated by a carbon monoxide-sensitive hydrogen sulfide pathway. *Proc Natl Acad Sci USA* **109**, 1293–1298.

6 Pandey AV and Fluck CE (2013) NADPH P450 oxidoreductase: structure, function, and pathology of diseases. *Pharmacol Ther* **138**, 229–254.

7 Iyanagi T, Xia C and Kim JJ (2012) NADPH-cytochrome P450 oxidoreductase: prototypic member of the diflavin reductase family. *Arch Biochem Biophys* **528**, 72–89.

8 Iyanagi T (2019) Molecular mechanism of metabolic NAD(P)H-dependent electron-transfer systems: the role of redox cofactors. *Biochim Biophys Acta Bioenerg* **1860**, 233–258.

9 Hamdane D, Xia C, Im SC, Zhang H, Kim JJ and Waskell L (2009) Structure and function of an NADPH-cytochrome P450 oxidoreductase in an open conformation capable of reducing cytochrome P450. *J Biol Chem* **284**, 11374–11384.

10 Sugishima M, Sato H, Higashimoto Y, Harada J, Wada K, Fukuyama K and Noguchi M (2014) Structural basis for the electron transfer from an open form of NADPH-cytochrome P450 oxidoreductase to heme oxygenase. *Proc Natl Acad Sci USA* **111**, 2524–2529.

11 Sugishima M, Wada K and Fukuyama K (2018) Recent advances in the understanding of the reaction chemistries of the heme catabolizing enzymes HO and BVR based on high resolution protein structures. *Curr Med Chem*. https://doi.org/10.2174/0929867326666181217142715

12 Wang M, Roberts DL, Paschke R, Shea TM, Masters BS and Kim JJ (1997) Three-dimensional structure of NADPH-cytochrome P450 reductase: prototype for FMN- and FAD-containing enzymes. *Proc Natl Acad Sci USA* **94**, 8411–8416.

13 Taira J, Sugishima M, Kida Y, Oda E, Noguchi M and Higashimoto Y (2011) Caveolin-1 is a competitive inhibitor of heme oxygenase-1 (HO-1) with heme: identification of a minimum sequence in caveolin-1 for binding to HO-1. *Biochemistry* **50**, 6824–6831.

14 Hayashi S, Omata Y, Sakamoto H, Hara T and Noguchi M (2003) Purification and characterization of a soluble form of rat liver NADPH-cytochrome P-450 reductase highly expressed in *Escherichia coli*. *Protein Expr Purif* **29**, 1–7.

15 Kabsch W (2010) XDS. *Acta Crystallographica Sect D Biol Crystallogra* **66**, 125–132.
16 Otwinowski Z and Minor W (1997) Processing of X-ray diffraction data collected in oscillation mode. *Methods Enzymol* **276**, 307–326.
17 Vagin A and Teplyakov A (1997) MOLREP: an automated program for molecular replacement. *J Appl Crystallogr* **30**, 1022–1025.
18 Collaborative Computational Project No. 4 (1994) The CCP4 suite: programs for protein crystallography. *Acta Crystallogr Sect D Biol Crystallogr* **50**, 760–763.
19 Emsley P, Lohkamp B, Scott WG and Cowtan K (2010) Features and development of Coot. *Acta Crystallogr Sect D Biol Crystallogr* **66**, 486–501.
20 Murshudov GN, Vagin AA and Dodson EJ (1997) Refinement of macromolecular structures by the maximum-likelihood method. *Acta Crystallogr Sect D Biol Crystallogr* **53**, 240–255.
21 Chen VB, Arendall WB 3rd, Headd JJ, Keedy DA, Immormino RM, Kapral GJ, Murray LW, Richardson JS and Richardson DC (2010) MolProbity: all-atom structure validation for macromolecular crystallography. *Acta Crystallogr D Biol Crystallogr* **66**, 12–21.
22 Aso Y, Gotoh S and Yamasaki N (2014) A HPLC method for simultaneous analysis of $NAD(P)^+$ and NAD(P)H — its application to the study of Spinach Ferredoxin: $NADP^+$ reductase-catalyzed transhydrogenation. *Agri Biol Chem* **53**, 1635–1639.
23 Grunau A, Paine MJ, Ladbury JE and Gutierrez A (2006) Global effects of the energetics of coenzyme binding: NADPH controls the protein interaction properties of human cytochrome P450 reductase. *Biochemistry* **45**, 1421–1434.
24 Xia C, Hamdane D, Shen AL, Choi V, Kasper CB, Pearl NM, Zhang H, Im SC, Waskell L and Kim JJ (2011) Conformational changes of NADPH-cytochrome P450 oxidoreductase are essential for catalysis and cofactor binding. *J Biol Chem* **286**, 16246–16260.